Two-color interband and intraband quantum well heterolaser

V. A. Kukushkin*
Institute of Applied Physics of RAS, 46 Ulyanov Street, 603950 Nizhny Novgorod, Russia
(Received 17 June 2008; published 30 September 2008)

A method of mid-infrared (ir) ($\lambda \simeq 50$ μm) generation at an intraband transition in interband optical ($\lambda \simeq 0.6$ μm) semiconductor quantum well (QW) heterolasers is considered. It is based on partial inversion of the intraband transition due to the electron population of its upper level, stimulated by a strong optical field simultaneously generated in the same device. In previous studies of the problem, the inhomogeneous broadening of this transition (i.e., its frequency dependence on the electron energies in the subbands that form it) was not taken into account. As a result, mid-ir generation was possible only under the condition of total (i.e., integrated over electron energies) inversion. In the present work it is shown that the inhomogeneous broadening of the intraband transition allows one to achieve mid-ir generation when it is inverted only in a narrow spectral range containing the interval where its interaction with the mid-ir mode has resonant character. At the same time, total inversion at this transition is absent. This circumstance makes it possible to significantly (by several times in comparison with previous estimates) reduce the threshold pumping current density for the start of mid-ir generation. As a result, this value proves to be in the experimentally achievable domain even at room temperature. This allows one to hope for the practical realization of a pulsed two-color optical and mid-ir laser based on a heterostructure with just one QW, employing simple and cheap injection pumping only, and working without any cooling.

DOI: 10.1103/PhysRevA.78.033838 PACS number(s): 42.55.Px

I. INTRODUCTION

The generation of powerful coherent mid-to far-infrared (ir) and terahertz (THz) radiation is an important problem of modern optics and laser physics due to its continuously growing employment in fundamental and applied research and various applications. Although there have been many different methods proposed so far to produce electromagnetic emission in this frequency range, low-dimensional semiconductor heterostructures [such as quantum wells (QWs) and quantum dots (QDs)] remain among the most efficient and convenient devices for such a purpose. This is attributed, primarily to the facts that, first, transition frequencies between their levels of dimensional quantization can be easily changed by adjusting the structure parameters and typically correspond to wavelengths from several to hundreds of micrometers and that, second, simple injection pumping may be employed for them.

Unfortunately, free-carrier absorption and diffraction of mid-to far-ir or THz radiation in such devices lead to strong nonresonant losses which rapidly rise with increase in the wavelength. This circumstance makes lasing in these structures possible only in the presence of a gain large enough to overcome losses. However, due to the very short lifetime of the excited state (which, as a rule, is comparable to or even shorter than that of the ground state), the maintenance of high cw population inversion at low-frequency laser intraband transitions in these devices is by no means an easy task. This problem can be solved, for example, by additional depletion of the ground state via tunneling in the superlattice as takes place in quantum cascade lasers (QCLs) [1–3]. But such devices are based on very complicated multilayer heterostructures and, as a rule, work under low temperatures. Another possibility to achieve high enough population inversion at the intraband transition is, obviously, the increase of its excited state lifetime. This can be done, for example, by making the frequency of this transition lower than the longitudinal optical (LO) phonon frequency and thereby suppressing electron transitions from the excited to the ground state with LO phonon emission. This scheme has been realized in fountain lasers (FLs) [4], which, however, like QCLs, work at low temperatures and, in addition, require complicated and expensive pumping by a CO_2 laser.

Because of these difficulties some researchers' attention has been drawn to an inversionless method of mid-to far-ir and THz field generation. In such schemes the latter is produced in the process of nonlinear difference-frequency mixing of two optical or near-ir fields with close frequencies, generated in low-dimensional heterostructure lasers (please see, for example, [5,6]). Although this method is based on a simple heterostructure with just one or several QWs and can work at room temperature, the second-order nonlinear susceptibility employed in it is rather small, so that the output mid-to far-ir or THz field power proves to be low.

There is, however, a simple scheme allowing one to obtain a high enough population inversion at an intraband laser transition (and, therefore, provide large output mid-to far-ir or THz power). This scheme, though probably not as efficient as QCLs or FLs, is based on a heterostructure with just one QW, can work at room temperature, and uses injection pumping only. In such a device the intraband laser transition is inverted due to the depletion of its lower-subband electron population, owing to stimulated electron-hole interband recombination in a strong optical or near-ir field. The latter is generated in the same structure at an interband transition. In previous studies of this scheme [7], however, only an intraband laser transition with no inhomogeneous broadening was considered. As a result, to provide mid-to far-ir or THz field amplification on it one had to ensure total (i.e., integrated over the electron quasimomenta in the QW plane) inversion

*vakuk@appl.sci-nnov.ru

between corresponding subbands. This led the author of [7] to the conclusion that the required pumping current density at room temperature would be too high and cause structural damage. To reduce it to experimentally reasonable values it was suggested in [7] to lower the structure temperature. But this certainly significantly diminished the attractiveness of such a scheme for applications.

Owing to these difficulties, later researchers' attention was directed to QD systems where, due to the phonon bottleneck effect, the lifetime of the upper lasing state can be increased by more than a hundred times in comparison with QWs even at room temperature [8], and inversion at the corresponding intraband transition can be easily obtained. However, the creation of samples with the high QD density necessary for fabrication of powerful heterolasers is a much more technologically difficult task than the production of QW heterostructures. It was proposed also to use a special funnel-like QW design [9] which allowed one to reduce the overlap between the electron wave functions in the upper and lower subbands. This led to the suppression of LO phonon emission and increase of the upper-subband lifetime, so that cw inversion at the intraband laser transition could be created. However, the small wave function overlap inevitably means the reduction of the intraband transition dipole moment, which results in low power of the output long-wavelength radiation.

But it is important to note that the intraband laser transition is, as a rule, inhomogeneously broadened so that its frequency depends on the electron quasimomenta in the QW plane. The cause of this inhomogeneous broadening is the difference in the electron effective masses in the different subbands forming the intraband transition. This difference can be as large as several tens of percent for the conduction band and can even reach several hundred percent for the valence band [10–12]. Certainly, the inhomogeneous broadening of the intraband transition complicates the theoretical model of the two-color laser considered, but also it allows one to amplify the mid-to far-ir or THz field at this transition when it is inverted only in a narrow range of electron quasimomenta comprising the interval where its frequency is resonant with that of the amplified mode. The absence of inversion at other electron quasimomenta does not lead to a significant long-wavelength field absorption as in this range the interaction between the amplified mode and transition is nonresonant and therefore inefficient. Moreover, as shown below, the amplification of a mid-to far-ir or THz field at the inhomogeneously broadened intraband transition is possible when there is no total inversion at it. In turn, this allows one to reduce significantly (by several times) the required pumping current density for the start of the mid-to far-ir or THz generation, J_{th}, in comparison with estimates in [7] where the existence of total inversion at the intraband transition was implied. As a result, even at room temperature J_{th} proves to be in an experimentally achievable domain. Since it allows cryogenic cooling to be dispensed with, this fact substantially increases the attractiveness of the present method of mid-to far-ir or THz generation for various applications, especially in biology and medicine.

The present paper is devoted to a detailed consideration of mid-ir generation in optical QW heterolasers with the inhomogeneous broadening of the low-frequency laser intraband transition consistently taken into account. In the next section a special design for a laser resonator for optical and mid-ir radiation is proposed and its optimal parameters are found. In Sec. III the interband generation of the optical modes is considered. In Sec. IV I study mid-ir intraband generation and find the corresponding threshold pumping current density J_{th}. In the Conclusion the main results of the paper most interesting for the practical realization of the scheme considered are outlined.

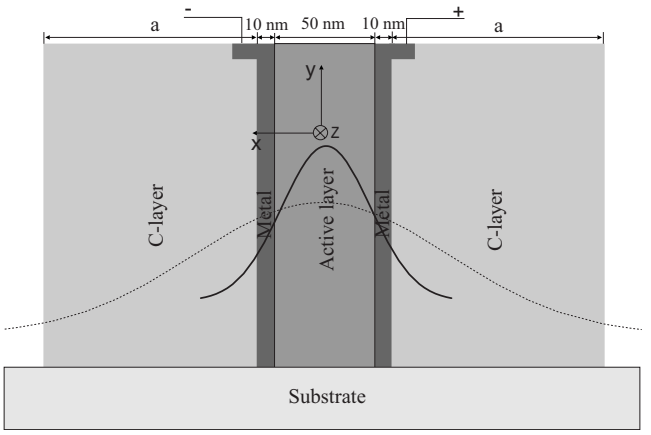

FIG. 1. Optical and mid-ir resonator for the two-color laser. Also shown are the coordinate system used in the text and qualitative sketches of the optical (thick solid line) and mid-ir (thin dashed line) mode intensity distributions along the structure growth direction x. z is the propagation direction.

II. OPTICAL AND MID-IR LASER RESONATOR DESIGN

Consider a slab dielectric waveguide (Fig. 1) consisting of an active layer (whose structure is specified in the next section), two very thin metallic layers (used for injection pumping) made of Ag,[1] and two thick C layers with low absorption in the optical and mid-ir regions. The thickness of both metallic layers is $\simeq$10 nm and is smaller than 20 nm, the thickness of the skin layer for both the optical (the vacuum wavelength $\lambda_O \simeq 0.6$ μm) and mid-ir ($\lambda_M \simeq 50$ μm) fields. As a result, they penetrate from the active layer to the C layers. The active and C layers serve as a dielectric waveguide for the optical radiation, whereas the C layers and surrounding air play the role of a dielectric waveguide for the mid-ir field.

It should be noted here that in Fig. 1 the waveguide is attached to the substrate by its lateral face. Such an untraditional orientation is employed here to use air as the cladding layers for the mid-ir field waveguide. The possibility of such a configuration is provided by the significant thickness of the C layers (please see below). But, if this orientation is an issue, one can use the standard one (i.e., when the structure growth axis x is orthogonal to the substrate) with teflon clad-

[1]The deposition of such thin metallic layers on a semiconductor surface is employed in the fabrication of waveguides for QCLs; please see, for example, [3,13,14].

ding layers (with low absorption in the mid-ir region) put above and below the C layers.

The structure end facets (orthogonal to the z axis) play the role of output mirrors for the optical radiation, whereas the mid-ir field is reflected from special Bragg mirrors deposited on either end facet [15,16]. As the typical value for the structure width in the y direction is ~ 100 μm and much larger than its thickness along the x axis, one can neglect the field variation along the y coordinate and consider this structure as a simple two-dimensional slab waveguide.

Let me represent the optical electric field $\mathbf{E}_O$ as a sum of TE modes

$$\mathbf{E}_O \equiv \frac{1}{2}\sum_n \tilde{\mathbf{E}}_n \exp(-i\omega_n t) + \text{c.c.}, \tag{1}$$

where

$$\tilde{\mathbf{E}}_n = \mathcal{E}_n \mathbf{e}_n \equiv \mathcal{E}(\omega_n)\mathbf{e}(\omega_n) \tag{2}$$

are the complex amplitudes of different longitudinal and transverse resonator modes n, and ω_n their generation frequencies. The mid-ir electric field $\mathbf{E}_M$ is represented by one TM mode,

$$\mathbf{E}_M \equiv \frac{1}{2}\tilde{\mathbf{E}}_M \exp(-i\omega_M t) + \text{c.c.}, \tag{3}$$

$$\tilde{\mathbf{E}}_M = \mathcal{E}_M \mathbf{e}_M. \tag{4}$$

The explicit expressions for $\mathbf{e}_n$ and $\mathbf{e}_M$ in Eqs. (2) and (4) describing the mode structures can be found, for example, in [17].

Under the parameters indicated in Fig. 1 the waveguiding structure supports the propagation of the lowest symmetric optical TE modes only so that all the modes $\tilde{\mathbf{E}}_n$ in Eq. (1) have the same type of transverse structure along the x axis. Their actual number at the high pumping current densities considered below can be as large as several hundred [18]. Numerical calculations show that in the proposed waveguide design the coefficient of their waveguide losses is $\alpha_O \simeq 840$ cm^{-1}. Such a large α_O is mainly determined by free-carrier absorption in the two thin metallic layers where the electric field of the optical TE modes, parallel to the y axis $\mathbf{E}_n \propto \cos[\sqrt{\omega_n^2 \epsilon_a(\omega_n)/c^2 - k_n^2}x]$, penetrates. Here c is the light velocity in vacuum, k_n the optical mode wave number along the propagation direction z, and $\epsilon_a(\omega_n)$ the active layer dielectric function.

The waveguide losses for the TM mid-ir field are also chiefly due to absorption in the metallic layers. However, the x component of the TM mode electric field in these layers is much smaller than its y component due to the boundary conditions on the dielectric-metal surface and the fact that at ω_M the absolute value of the metal dielectric function is much larger than that of the active or C layers. So the mid-ir TM mode waveguide losses are mainly determined by the y component of its electric field, $\tilde{E}_{My}$. But, in contrast to the field of TE optical modes, $\tilde{E}_{My}$ is proportional to $\sin[\sqrt{\omega_M^2 \epsilon_a(\omega_M)/c^2 - k_M^2}x]$ where k_M is the mid-ir wave number along z. So $\tilde{E}_{My}$ is rather low at small $|x|$ where the metallic layers are placed. The value of k_M grows with the increase of the C layer thickness a, so that the larger the latter, the lower are the mid-ir mode losses. The actual value of a is obviously determined by the technological possibility of growing thick carbon films. So, taking $a=14$ μm for numerical calculations, it is easy to obtain the result that in such a case the mid-ir waveguide losses $\alpha_M \simeq 0.02$ cm^{-1}.

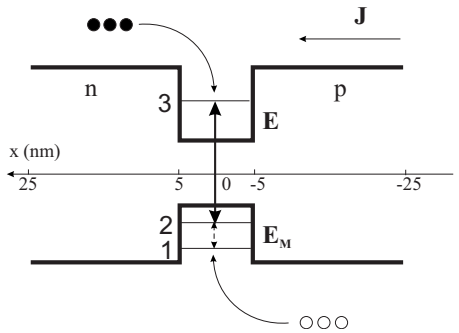

FIG. 2. Conduction and valence band edges for an $Al_{0.37}Ga_{0.63}As$ QW surrounded by symmetric $Al_{0.43}Ga_{0.57}As$ barriers. The optical generation occurs at the interband transition $3 \rightarrow 2$ (solid arrow) and the mid-ir generation at the intraband transition $2 \rightarrow 1$ (dashed arrow) with injection pumping providing the necessary inversion. Filled circles denote electrons and empty ones holes.

III. OPTICAL INTERBAND GENERATION

The complex amplitudes of optical modes can be found from equations obtained in the standard theory of resonator excitation [19]:

$$\mathcal{E}_n = -\frac{4\pi i \omega_n \int \tilde{\mathbf{j}}_n \mathbf{e}_n dV}{(\omega_n^2 - \omega_{k_n}^2)\int \epsilon(\omega_n)\mathbf{e}_n^2 dV}. \tag{5}$$

Here $\tilde{\mathbf{j}}_n$ is the complex amplitude of the exciting current density at the frequency ω_n averaged over the QW thickness $l \simeq 10$ nm, $\omega_{k_n} = \omega'_{k_n} + i\omega''_{k_n}$ the eigenmode frequencies, and $\epsilon(\omega_n)$ the structure dielectric function (depending on x). The use of the averaged current density in Eq. (5) [and in Eq. (25) below] is valid as the optical and mid-ir mode variations over l are negligible. To find $\tilde{\mathbf{j}}_n$ it is necessary to specify the active layer composition.

As was mentioned in the Introduction, the inhomogeneous broadening of intraband laser transitions in the valence band can be much larger than in the conduction band. So, for the present purpose, it is advantageous to use an intraband transition in the valence band. Such a transition can be formed in an active layer consisting of one undoped 10-nm-wide $Al_{0.37}Ga_{0.63}As$ QW surrounded by two 20-nm-thick $Al_{0.43}Ga_{0.57}As$ barriers (Fig. 2). The left and right barriers are, respectively, n and p doped at the same level $\sim 10^{16}$ cm^{-3} except for the parts adjacent to the QW of thickness of the order of the carrier penetration depth, which is estimated to be ~ 2.3 nm for the present heterostructure. Such modulation doping is necessary to avoid undesirable

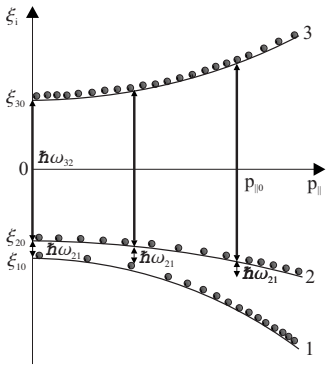

FIG. 3. Schematic of subband electron energies as functions of $p_\|$ near the Γ point in the $Al_xGa_{1-x}As$ heterosystem. Subbands 1 and 2 in the valence band are the two highest heavy-hole subbands, and subband 3 the only electronic subband in the conduction band. Optical generation occurs at the interband transition $3 \rightarrow 2$ in the interval $0 < p_\| < p_{\|0}$. Filled circles denote electrons.

carrier scattering with barrier states. Assuming a 60:40 band offset and using the well-known approximation for the $Al_xGa_{1-x}As$ Γ-point direct band gap dependence on the Al mole fraction x at room temperature [20], it is easy to show that in a QW with such parameters only one level of dimensional quantization (level 3 in Fig. 2) is formed in the conduction band [21]. Due to electron motion in the QW plane, each level in Fig. 2 is a subband, i.e., a set of electronic states with different energies ξ_i $(i=1,2,3)$ depending (in the isotropic effective mass approximation used here) only on the electron quasimomentum in the QW plane, $p_\| \equiv \sqrt{p_y^2+p_z^2}$: $\xi_i \simeq \xi_{i0}+p_\|^2/(2m_i)$, where m_i are the electron effective masses (Fig. 3). The frequency ω_{32} of the interband transition $3 \rightarrow 2$ at $p_\|=0$ corresponds to the vacuum wavelength $\lambda \simeq 0.6$ μm (optical field), whereas the frequency ω_{21} of the intraband transition $2 \rightarrow 1$ at $p_\|=0$ is equivalent to $\lambda_M \simeq 50$ μm (mid-ir field).

The interaction of such a system with an electromagnetic field is described by the von Neumann equation [22] for its density matrix ρ_{ij} depending (in the isotropic approximation employed here) only on $p_\|$ or, which is the same, on the detuning Δ of the frequency of the transition $3 \rightarrow 2$ from its value ω_{32} at $p_\|=0$: $\Delta \equiv p_\|^2(m_2-m_3)/(2\hbar m_2 m_3)$ $(m_{1,2}<0,\ m_3>0)$. Using the standard representation of the nondiagonal density matrix elements as products of slowly varying amplitudes $\tilde{\rho}_{32n}$, $\tilde{\rho}_{31n}$, and $\tilde{\rho}_{21}$ with oscillating exponential factors with frequencies ω_n, $\omega_n+\omega_M$, and ω_M, respectively, $\tilde{\mathbf{j}}_n$ can be represented as [21]

$$\tilde{\mathbf{j}}_n = -i\omega_n \mathbf{d}_{32} \sin(k_n z) \int_0^{+\infty} N\tilde{\rho}_{32n} d\Delta/l. \tag{6}$$

Here the identity $m_0[\hat{H},\mathbf{r}]/\hbar^2=\boldsymbol{\nabla}$ (where m_0 is the free-electron mass, $\hat{H}$ is the electron Hamiltonian, and $\boldsymbol{\nabla} \equiv \partial/\partial\mathbf{r}$) is used, $\mathbf{d}_{32}=e\mathbf{z}_{32}$ is the dipole moment of transition $3 \rightarrow 2$, determined by the elementary charge e and the transition matrix element $\mathbf{z}_{32}$, and N is the effective QW density of states for which a simple calculation gives the formula

$$N \simeq m_2 m_3/[2\pi\hbar(m_2-m_3)]. \tag{7}$$

The values $\tilde{\rho}_{32n}$, $\tilde{\rho}_{31n}$, and $\tilde{\rho}_{21}$ are determined from the system of equations [22]

$$d\tilde{\rho}_{32n}/dt + \Gamma_{32}\tilde{\rho}_{32n} = ie_n n_{23} + ie_M^* \tilde{\rho}_{31n},$$

$$d\tilde{\rho}_{31n}/dt + \Gamma_{31}\tilde{\rho}_{31n} = -ie_n \tilde{\rho}_{21} + ie_M \tilde{\rho}_{32n},$$

$$d\tilde{\rho}_{21}/dt + \Gamma_{21}\tilde{\rho}_{21} = ie_M n_{12} - i\sum_n e_n^* \tilde{\rho}_{31n}, \tag{8}$$

where n_{ij}, $i,j=1,2,3$, are the time-independent (and, therefore, main) contributions to the population differences $\rho_{ii}-\rho_{jj}$, $e_n=\mathcal{E}_n \mathbf{d}_{32}\bar{\mathbf{e}}_n(0)/(2\hbar)$ and $e_M=\mathcal{E}_M \mathbf{d}_{21}\bar{\mathbf{e}}_M(0)/(2\hbar)$ are the optical and mid-ir Rabi frequencies, and $\bar{\mathbf{e}}_n(x)$ and $\bar{\mathbf{e}}_M(x)$ are the transverse distributions of the optical and mid-ir modes [17],

$$\Gamma_{32} = \gamma_{32} + i(\omega_{32}+\Delta-\omega_n),$$

$$\Gamma_{31} = \gamma_{31} + i[\omega_{31}+(1+\eta)\Delta-\omega_n-\omega_M],$$

$$\Gamma_{21} = \gamma_{21} + i(\omega_{21}+\eta\Delta-\omega_M). \tag{9}$$

where

$$\eta = m_3(m_2-m_1)/[m_1(m_3-m_2)], \tag{10}$$

γ_{21}, γ_{31}, and γ_{32} are phenomenological relaxation rates for the nondiagonal density matrix elements, and, due to the randomness of the optical mode mutual phases, here and in what follows all cross terms are dropped in summations over them. The values γ at the QW sheet carrier densities considered below are determined mainly by emission or absorption of LO phonons [23] and intrasubband carrier-carrier scattering [24] and for estimates can be taken even and approximately equal to $\gamma \equiv 10^{13}$ s^{-1}. In regard to this estimate of γ, it is necessary to note here that J_{th} rises with the increase of γ, but not very quickly. According to numerical simulations, the growth of γ by two times (from 10^{13} to 2×10^{13} s^{-1}) leads to the enhancement of J_{th} by 1.45 times only, in comparison with the estimate obtained in Sec. IV for $\gamma=10^{13}$ s^{-1}. So, even in the case of moderate deviation of the actual γ from the value of 10^{13} s^{-1} used here, J_{th} may still remain in the experimentally achievable domain. Moreover, the quite probable increase of the actual intersubband equilibration time τ_{21} in comparison with the estimate given for it [please see the discussion in the footnote after Eq. (20) below] leads to the reduction of J_{th} below the value obtained in Sec. IV. This effect can quite well compensate for the moderate increase of J_{th} due to the growth of γ so that the resulting J_{th} will be of the order of or even smaller than the value quoted in Sec. IV.

The appearance of parameter η in (9) reflects the difference of the electron effective masses in the second and first subbands, which leads to its being nonparallel, i.e., to the dependence of the transition $2 \rightarrow 1$ frequency on $p_\|$ (please see Fig. 2 which is drawn for the AlGaAs heterosystem where $|m_2|>|m_1|$ [10,11]).

The stationary solution of (8) for $\tilde{\rho}_{32n}$ (obtained near the mid-ir generation threshold where one can neglect small terms proportional to e_M^2) takes the form

$$\tilde{\rho}_{32n} \simeq ie_n n_{23}/\Gamma_{32}, \tag{11}$$

where

$$n_{23} = \frac{\bar{n}_{23}}{1 + 4(\gamma/r)\Sigma_n |e_n|^2/|\Gamma_{32}|^2} \tag{12}$$

is the stationary solution of the equation [22]

$$dn_{23}/dt + r(n_{23} - \bar{n}_{23}) = -4\ \mathrm{Im} \sum_n e_n^* \tilde{\rho}_{32n} \tag{13}$$

with r being the relaxation rate of n_{23} to its equilibrium value $\bar{n}_{23}$. Actually, in Eq. (13) only relaxation processes connected with intrasubband redistribution of carriers owing to intrasubband carrier-carrier scattering and emission or absorption of LO phonons are taken into account. As was mentioned above, the same phenomena determine the nondiagonal density matrix element relaxation rate γ so that $r \sim \gamma$. Here it is necessary to note that these intraband processes lead to the thermalization of carriers in subbands with fixed carrier number and mean energy in each of them. The intersubband carrier energy exchange and transitions accounting for the equilibration between different subbands proceed on a much longer time scale [25] and therefore can result only in small corrections to the relaxation term in Eq. (13). But it is these processes that determine the stationary carrier sheet density in each subband under injection pumping and optical generation and, therefore, the equilibrium differences of subband populations $\bar{n}_{ij}$ (please see below).

For the following estimations it is valid to neglect the small shift of the optical mode generation frequencies from the real parts of the corresponding resonator eigenfrequencies, i.e., to put $\omega_n \simeq \omega'_{k_n}$ and $\omega_M \simeq \omega'_{k_M}$. For a heterolaser length along the z axis of $\simeq 2.2$ cm (please see Sec. IV) the spectral spacing between different longitudinal optical modes is much smaller than the homogeneous $3 \to 2$ linewidth γ. All the more, it is much smaller than the scale of $|e_n|$ variation with ω_n which, according to the final formula (14), cannot be less than the analogous value for $\bar{n}_{23}(\omega_n - \omega_{21})$, i.e., $k_B T/\hbar \simeq 4\gamma$, where $T \simeq 300$ is the structure temperature and k_B the Boltzmann constant. As a result, one can replace the summation over modes in (12) with integration and neglect the variations of $|e_n|$ and $\bar{n}_{23}$ over a frequency interval $\sim \gamma$. Then, from Eqs. (5), (6), (11), and (12), it is easy to obtain an equation for the optical mode complex amplitudes in the form

$$|e(\omega_n)|^2 = \frac{r}{4\pi D(\omega_n)} \left(\frac{\bar{n}_{23}(\Delta)}{n_{23}(\Delta)} - 1 \right), \tag{14}$$

where

$$n_{23}(\Delta) = \begin{cases} n_N, & \Delta < \Delta_{\max}, \\ \bar{n}_{23}(\Delta), & \Delta > \Delta_{\max}, \end{cases} \tag{15}$$

$\Delta_{\max} \equiv p_{\|0}^2 (m_2 - m_3)/(2\hbar m_2 m_3)$, $\bar{n}_{23}(\Delta_{\max}) = n_N$, $D(\omega_n) \equiv D_n$ is the mode spectral density, $\omega_n = \omega_{32} + \Delta$, and

$$n_N = \frac{\hbar \omega''_{k_n} \mathrm{Re}\left[\int \epsilon(\omega_n) \bar{\mathbf{e}}_n^2 dx \right]}{\pi^2 \omega_n |\mathbf{d}_{23} e_n(0)|^2 N}. \tag{16}$$

Here ω''_{k_n} can be estimated as $0.5\alpha_n v_n$ where $v_n \equiv \partial \omega'_{k_n}/\partial k_n$ is the optical group velocity. From (15) it is clear that, according to the standard theory of field amplification in active media with homogeneous broadening [26], in the whole frequency interval of transition $3 \to 2$ where the optical generation occurs the difference between subband 3 and 2 populations is approximately equal to its threshold value n_N and the mode intensity is proportional to $\bar{n}_{23}(\omega_n - \omega_{32}) - n_N$.

Now, it is necessary to connect $\bar{n}_{23}$ in Eq. (14) with the pumping current density J. This can be done using the following considerations. The equilibrium differences of the subband populations, $\bar{n}_{ij} \equiv \bar{\rho}_{ii} - \bar{\rho}_{jj}$, are determined by the diagonal elements of the equilibrium density matrix $\bar{\rho}_{ii}$, given by Fermi distributions (where the spin index is omitted for brevity)

$$\bar{\rho}_{ii} = 1 \Big/ \left[\exp\left(\frac{\xi_{i0} + p_\|^2/(2m_i) - \mu_i}{k_B T} \right) + 1 \right]. \tag{17}$$

Here the chemical potentials μ_i are functions of the hole sheet densities in subbands 1 and 2, ρ_{h1} and ρ_{h2}, and the electron sheet density in subband 3, ρ_{e3} (where $\rho_{h1} + \rho_{h2} \simeq \rho_{e3}$ due to quasineutrality), found from the following equations:

$$\rho_{hi} = -\frac{k_B T}{\pi \hbar^2} m_i \ln\left[1 + \exp\left(\frac{\xi_{i0} - \mu_i}{k_B T} \right) \right], \tag{18}$$

$i = 1, 2$, and

$$\rho_{e3} = \frac{k_B T}{\pi \hbar^2} m_3 \ln\left[1 + \exp\left(\frac{\mu_3 - \xi_{30}}{k_B T} \right) \right], \tag{19}$$

obtained by the integration of Eq. (17) over $2\pi p_\| dp_\|/(2\pi\hbar)^2$ and summation over hole or electron spin projections.

The values ρ_{h1} and ρ_{h2}, in turn, can be expressed through the total sheet hole density in subbands 1 and 2, $\rho_h \equiv \rho_{h1} + \rho_{h2}$. To do so let me note that ρ_{h1} is determined by the stationary solution of the equation

$$d\rho_{h1}/dt = -\rho_{h1}/\tau_{31} + J/(2e) - (\rho_{h1} - \bar{\rho}_{h1})/\tau_{21}, \tag{20}$$

where the term $-\rho_{h1}/\tau_{31}$ (with $\tau_{31} \simeq \tau_{32} \sim \tau \equiv 1$ ns) is responsible for ρ_{h1} reduction due to spontaneous recombination with electrons in the third subband, the term $J/(2e)$ for its increase owing to pumping current (where the factor $1/2$ takes into account the fact that only one-half of J is thanks to hole motion), and the term $-(\rho_{h1} - \bar{\rho}_{h1})/\tau_{21}$ (with $\tau_{21} \sim 1$ ps [27,28]) for the process of equilibration between subbands 1 and 2 accompanied by LO phonon emission or absorption.[2] Here $\bar{\rho}_{h1}$ is the hole sheet density in the first subband that

[2]It is necessary to note here that this estimate of τ_{21} does not take into account effects of Fermi degeneracy and Pauli blocking. These effects at high QW carrier sheet densities $\rho_h \sim \rho_{e3}$ considered below can increase τ_{21} above a value of 1 ps (please see, for example, [25]). Thus, as J_{th} decreases with the increase of τ_{21}, the estimate of J_{th} obtained in Sec. IV for $\tau_{21} = 1$ ps can somewhat overvalue J_{th}.

would occur if complete equilibrium between subbands 1 and 2 took place, i.e., if they were characterized by the same chemical potential μ_0, determined by ρ_h through the equation

$$\rho_h = -\frac{k_B T}{\pi\hbar^2}\left\{ m_1 \ln\left[1+\exp\left(\frac{\xi_{10}-\mu_0}{k_B T}\right)\right] + m_2 \ln\left[1+\exp\left(\frac{\xi_{20}-\mu_0}{k_B T}\right)\right]\right\}, \tag{21}$$

so that

$$\bar{\rho}_{h1} = -\frac{k_B T}{\pi\hbar^2} m_1 \ln\left[1+\exp\left(\frac{\xi_{10}-\mu_0}{k_B T}\right)\right]. \tag{22}$$

From (20) it is easy to find that

$$\rho_{h1} = \frac{\tau\tau_{21}}{\tau_{21}+\tau}[\bar{\rho}_{h1}/\tau_{21} + J/(2e)], \tag{23}$$

and ρ_{h2} is given by an obvious formula $\rho_{h2}=\rho_h-\rho_{h1}$. As, according to Eqs. (21) and (22), $\bar{\rho}_{h1}$ is a function of ρ_h, this solves the above-mentioned task of expressing ρ_{h1} and ρ_{h2} through ρ_h.

Then it is easy to show that ρ_h itself depends on J according to the balance equation

$$2N\,\mathrm{Re}\int_0^{\Delta_{\max}}\int_{\omega_{32}}^{\omega_{32}+\Delta_{\max}} \frac{n_{23}(\Delta)D_n|e_n|^2}{\Gamma_{32}} d\omega_n d\Delta - \rho_h/\tau + J/(2e) = 0, \tag{24}$$

where the first term describes the reduction of ρ_h due to recombination of electrons in subband 3 with holes in subband 2 induced by the strong optical field, the second term the reduction of ρ_h owing to spontaneous recombination of holes in the first and second subbands with electrons in the third subband, and the last term the increase of ρ_h thanks to the pumping current. Thus, numerical solution of Eqs. (17)–(24) allows one to find $\bar{n}_{23}$ (and $\bar{n}_{12}$ which will be used in the next section) as a function of J.

IV. MID-IR INTRABAND GENERATION

The condition for the start of the mid-ir generation can be found from equations similar to Eqs. (5) and (6):

$$\mathcal{E}_M = -\frac{4\pi i\omega_M \int \tilde{\mathbf{j}}_M \mathbf{e}_M dV}{(\omega_M^2-\omega_{k_M}^2)\int \epsilon(\omega_M)\mathbf{e}_M^2 dV}, \tag{25}$$

$$\tilde{\mathbf{j}}_M = -i\omega_M \mathbf{d}_{12}\sin(k_M z)\int_0^{+\infty} N\tilde{\rho}_{21} d\Delta/l, \tag{26}$$

where $\omega_{k_M}=\omega'_{k_M}+i\omega''_{k_M}$ is the complex eigenfrequency of the mid-ir mode. By analogy with the optical field ω''_{k_M} can be estimated as $0.5(\alpha_M+\alpha_{\mathrm{MR}})v_M$ where α_{MR} is responsible for the losses connected with the output mirrors ($\alpha_{\mathrm{MR}} \sim 0.1\ \mathrm{cm}^{-1}$ for highly reflective mid-ir Bragg mirrors with a reflection coefficient $\gtrsim 80\%$ [15,16] and structure length $\simeq 2.2$ cm) and $v_M \equiv \partial\omega'_{k_M}/\partial k_M$ is the mid-ir group velocity.

Aiming at determining the threshold of the mid-ir generation, it is sufficient to find $\tilde{\rho}_{21}$ with accuracy up to terms proportional to the mid-ir field in the first power only. Simple calculation making use of Eqs. (8) gives [5]

$$\tilde{\rho}_{21} \simeq ie_M\left(\frac{n_{12}}{\tilde{\Gamma}_{21}} + \frac{n_{23}}{\tilde{\Gamma}_{21}}\int_{\omega_{32}}^{\omega_{32}+\Delta_{\max}} \frac{D_n|e_n|^2}{\Gamma_{32}\Gamma_{31}} d\omega_n\right), \tag{27}$$

where

$$\tilde{\Gamma}_{21} = \Gamma_{21} + \int_{\omega_{32}}^{\omega_{32}+\Delta_{\max}} D(\omega_n)|e(\omega_n)|^2 d\omega_n/\Gamma_{31}. \tag{28}$$

The first term in (27) describes one-photon absorbtion or amplification proportional to the population difference n_{12} at transition $2\to 1$. The second term is responsible for the parametric interaction of the optical modes with the mid-ir mode and arises from the product $e_n^*\tilde{\rho}_{31n}$ in (8) describing the mixing of the optical field with the polarization at transition $3\to 1$. The letter is excited due to the two-photon process $\tilde{\rho}_{31n} \propto e_M\tilde{\rho}_{32n} \propto e_M e_n n_{23}$.

The population difference n_{12} entering Eq. (27) can be found from the following considerations. Writing the equation for n_{13} [22],

$$dn_{13}/dt + r(n_{13}-\bar{n}_{13}) = -2\,\mathrm{Im}\sum_n e_n^*\tilde{\rho}_{32n} \tag{29}$$

(where it is assumed for estimations that the relaxation rate of the population difference at transition $3\to 1$ to its equilibrium value is the same as at transition $3\to 2$) and combining it with (13), it is easy to show that in a stationary situation $n_{13}=\bar{n}_{13}+(n_{23}-\bar{n}_{23})/2$. From here it follows that

$$n_{12} \equiv n_{13}-n_{23} \equiv \bar{n}_{13} - \frac{n_{23}+\bar{n}_{23}}{2} \equiv \bar{n}_{12} - \frac{n_{23}-\bar{n}_{23}}{2}. \tag{30}$$

So n_{12} is expressed through n_{23} determined in Eq. (15).

Substituting Eq. (27) in Eq. (26) and Eq. (26) in Eq. (25), it is easy to obtain a condition that has to be satisfied at the threshold of mid-ir generation:

$$\mathrm{Re}\int_0^{+\infty}\left(\frac{rn_{23}}{4\pi\tilde{\Gamma}_{21}}\int_0^{\Delta_{\max}}\frac{\bar{n}_{23}(\Delta')-n_N}{n_N\Gamma_{31}\Gamma_{32}}d\Delta' + \frac{n_{12}}{\tilde{\Gamma}_{21}}\right)d\Delta = n_M, \tag{31}$$

where

$$n_M = \frac{\hbar\omega''_{k_M}\mathrm{Re}\left[\int \epsilon(\omega_M)\bar{\mathbf{e}}_M^2 dx\right]}{\pi\omega_M|\mathbf{d}_{12}e_M(0)|^2 N}, \tag{32}$$

$\mathbf{d}_{12}=e\mathbf{z}_{12}$ is the dipole moment of transition $2\to 1$, determined by the elementary charge e and the transition matrix element $\mathbf{z}_{12}$, and $\bar{\mathbf{e}}_M(x)$ is the transverse mid-ir mode distribution.

For the parameters cited above and typical $z_{32}=1$ nm and $z_{12}=5$ nm [29,30] $n_N \simeq -0.75$ and $n_M \simeq -0.25$ so that, as follows from its numerical analysis, Eq. (31) is satisfied at $J=J_{\mathrm{th}} \simeq 100\ \mathrm{kA/cm}^2$. Although rather high, this pumping current density is quite achievable at room temperature in the

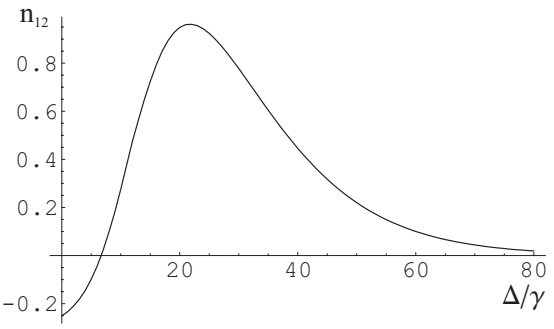

FIG. 4. Dependence of n_{12} on Δ/γ. The optical generation occurs in the interval $0<\Delta/\gamma<\Delta_{\max}/\gamma\simeq 12$.

pulsed regime (please see, for example, [18]). The value n_{12} as a function of Δ for the parameters used above is depicted in Fig. 4. From it one can see that inversion at the transition $2\rightarrow 1$ exists only for $0<\Delta<6.5\gamma$ (or, which is the same, $0<p_{\|}<0.7p_{\|0}$) due to electron transitions from the third to the second subband induced by the optical field. But the frequency of this transition, $\omega_{21}+p_{\|}^2(m_1-m_2)/(2\hbar m_1 m_2)\equiv\omega_{21}+\eta\Delta$, also varies with Δ. According to the results of [10], $m_1\simeq -0.05m_0$, $m_2\simeq -0.14m_0$, and $m_3\simeq 0.07m_0$ so that $\eta\simeq 0.6$ [Eq. (10)]. Therefore, the mid-ir field with frequency ω_{21} interacts with the transition $2\rightarrow 1$ efficiently only in the interval $0<\Delta\lesssim 1.5\gamma$ (or, which is the same, $0<p_{\|}<0.4p_{\|0}$), where its frequency exceeds ω_{21} by not more than the homogeneous linewidth γ. According to what has just been said, in all this interval the transition $2\rightarrow 1$ is inverted so that efficient mid-ir field amplification takes place here. In most of the remaining interval $1.5\gamma<\Delta$ the transition $2\rightarrow 1$ is not inverted (Fig. 4), but its frequency here is bigger than ω_{21} by more than the homogeneous linewidth γ. Thus, the mid-ir field interaction with the transition $2\rightarrow 1$ is inefficient here so that its absorption at $1.5\gamma<\Delta$ is rather weak. Therefore, upon the whole, the mid-ir field amplification at transition $2\rightarrow 1$ should take place. Numerical simulations of Eq. (31) show that this is indeed the case for the parameters chosen.

It is important to stress here that this amplification occurs when $N\int_0^{+\infty} n_{12}d\Delta\simeq 1.7\times 10^{12}$ cm^{-2} is positive so that the transition $2\rightarrow 1$ as a whole is still far away from being inverted. The latter conclusion can also be proved by the following simple considerations. From numerical calculations it follows that under the parameters used the threshold pumping current density for the start of optical generation is $J_0\simeq 500$ A/cm^2. Then, the condition of attaining total inversion at the transition $2\rightarrow 1$ can be written as [7]

$$\tau J_0/J<\tau_{21}, \tag{33}$$

where $\tau J_0/J$ is the time of $3\rightarrow 2$ electron-hole recombination induced by the optical field [31]. Thus, for $J=J_{\text{th}}\simeq 100$ kA/cm^2 the condition (33) is not satisfied as its left-hand side (LHS) is $\simeq 5$ times larger than its RHS, so that, in accordance with numerical analysis, there is no total inversion at the transition $2\rightarrow 1$.

The possibility to amplify the mid-ir field at the transition $2\rightarrow 1$ in the absence of total inversion at it, in turn leads to a significant (by several times) decrease of the estimated threshold pumping current density for the start of mid-ir generation, J_{th}, in comparison with the results of [7], where the inhomogeneous broadening of transition $2\rightarrow 1$ was not taken into account. It allows one to put J_{th} into an experimentally achievable range even at room temperature and therefore substantially increase the attractiveness of such a two-color optical and mid-ir laser for various applications.

It is important to note here that, as $\omega_{32}+\Delta_{\max}>\omega_{31}$, the optical modes could in principle cause not only $3\rightarrow 2$, but also $3\rightarrow 1$ electron transitions. This effect, however, is undesirable as it would lead to the additional population of the first subband by the electrons from the third subband and, therefore, the reduction or even complete disappearance of partial inversion at the transition $2\rightarrow 1$. But in the symmetric heterostructures (i.e., structures with the same heights and widths of the left and right barriers around the QW) considered here (Fig. 2) the $3\rightarrow 1$ dipole moment is zero. So stimulated $3\rightarrow 1$ electron transitions are strongly suppressed and can be neglected. Certainly, there is another possibility for the undesirable population of the first subband: it could be filled due to the optical field inducing electron transitions from subbands lying above the third subband. To avoid this process it is necessary to use a shallow QW where (as was explained in Sec. III) just one subband (designated here as the third subband) is formed in the semiconductor conduction band. In such a structure these transitions are impossible simply owing to the absence of subbands above the third subband.

It is worth mentioning also that Eq. (31) takes into account the mid-ir field amplification not only due to partial inversion at the transition $2\rightarrow 1$ [for which the second term in Eq. (31) is responsible], but also due to parametric interaction with the optical modes [the first term in Eq. (31)]. But numerical calculations show that the ratio of the first term to the second is $\lesssim 0.1$ so that the inversionless mechanism of the mid-ir amplification [32] proves to be much weaker than the inversion mechanism. The cause of this is the small value of the integral over Δ' in the first term of Eq. (31), i.e., the significant mutual compensation of different optical modes contributions to the parametric mid-ir radiation amplification.

In conclusion of this section it is necessary to note that at such high $J_{\text{th}}\simeq 100$ kA/cm^2 the corresponding carrier sheet density in the QW, $\rho_h\sim\rho_{e3}$, proves also to be large and (as follows from the numerical analysis) approximates to 5×10^{12} cm^{-2}. Although this and even larger sheet densities are quite achievable experimentally (please see, for example, [18]), the carrier-carrier interaction at this $\rho_h\sim\rho_{e3}$ can in principle lead to a noticeable shift of the transition $2\rightarrow 1$ frequency due to the depolarization effect [33]. The physical cause of the latter is that the actual complex amplitude of the mid-ir field acting on the electrons and holes in the QW differs from $\tilde{\mathbf{E}}_M/2$. This difference can be determined as follows. As the y component of the TM-mode mid-ir electric field in the QW is zero, only its x component is responsible for interaction with carriers in the QW. Then, its local value in the QW, $\tilde{E}_{Mlx}/2$, is determined from the formula $\epsilon_{\text{QW}}\tilde{E}_{Mlx}/2=\epsilon_a(\omega_{21})\tilde{E}_{Mx}/2$ following from the boundary condition at the QW-barrier interface. Here ϵ_{QW} is the dielectric

function inside the QW, which can be expressed as the sum of the active layer dielectric function $\epsilon_a(\omega_{21})$, and the contribution due to the QW carriers. The latter can be approximated by a simple formula $4\pi i\sigma_{xx}/\omega_M$, where σ_{xx} is the conductivity due to QW carriers, averaged over the QW width and $\sigma_{xx} \equiv d_{21x}\tilde{j}_{Mx}/(\hbar e_M)$. Then, it is easy to show that this difference between $\tilde{E}_{Mlx}/2$ and $\tilde{E}_{Mx}/2$ results in the appearing of an additional factor

$$\left(\frac{\varepsilon_a(\omega_{21})}{\varepsilon_a(\omega_{21}) + \dfrac{4\pi\omega_{21}N|d_{21x}|^2 \displaystyle\int_0^{+\infty} \tilde{\rho}_{21} d\Delta}{\hbar\omega_M l e_M}} \right)^2 \tag{34}$$

after the function Re in Eq. (31).

Regarding ω_M as a free parameter, one can investigate Eq. (31) numerically both without and with this additional factor. As a result, it can be shown that in these two cases the minima of the LHS of Eq. (31) lie at $\omega_M \simeq \omega_{21} + \gamma$ and differ from each other by a value $\lesssim\gamma$. So [keeping in mind that the RHS of Eq. (31) $n_M < 0$], one can conclude that with increasing J the mid-ir generation in these two cases for the first time will take place at close frequencies separated by a value $\lesssim\gamma$. Thus, as $\gamma/\omega_{21} \simeq 0.3 \ll 1$, the depolarization effect leads to only a small relative shift of the frequency of transition $2 \to 1$. It means that the simple three-level scheme that is employed here and that neglects many-body effects arising due to carrier-carrier interaction can give a qualitatively true description of the physical system investigated.[3] The cause of such a moderate depolarization shift of the mid-ir resonance frequency is the above-mentioned strong inhomogeneous broadening of transition $2 \to 1$. This leads to a situation when only a small part of the total number of holes in subbands 2 and 1 (namely, the holes in the interval of $p_\parallel$ where the frequency of transition $2 \to 1$ differs from ω_M by a value $\lesssim\gamma$) contributes to $\tilde{j}_M$. Therefore, $\sigma_{xx} \propto \tilde{j}_M$ proves to be rather small so that the difference between the dielectric functions inside and outside the QW turns out to be quite moderate.

[3] As to the band gap renormalization due to many-body effects, in [34] it is shown that in $Al_xGa_{1-x}As$ solid solutions for carrier densities corresponding to those considered here the band gap energy changes by $\simeq 4\%$ only. So this effect can be neglected for estimates made in the present work.

V. CONCLUSION

In conclusion, it is shown that a two-color interband and intraband QW heterolaser can operate not only under cryogenic cooling, but also without any cooling at all. The latter regime becomes possible if three conditions are satisfied. First, one has to employ the special waveguide design described above, which, though leading to rather strong absorption of the optical radiation, provides low losses for the mid-ir field. Second, it is necessary to use a shallow symmetric QW where just one level of dimensional quantization is realized in the conduction band. And third, the intraband transition for the mid-ir generation should lie in the valence band where electron effective masses in different subbands can significantly vary from each other.

The estimates made show that under these three conditions it is possible to create a pulsed two-color optical and mid-ir heterolaser based on rather an elementary structure with just one QW, using simple and cheap injection pumping only, and working at room temperature.

ACKNOWLEDGMENTS

This research was supported by RFBR (Grant No. 07-02-00486) and the Council for Support of the Leading Scientific Schools in Russia (Grant No. 4485.2008.2).

[1] J. Faist, F. Capasso, D. L. Sivco, C. Sirtori, A. L. Hutchinson, and A. Y. Cho, Science **264**, 553 (1994).
[2] F. Capasso, C. Gmachl, A. M. Tredicucci, A. L. Hutchinson, D. L. Sivco, and A. Y. Cho, Opt. Photonics News **10**, 33 (1999).
[3] S. Dhillon, J. Alton, S. Barbieri, C. Sirtori, A. de Rossi, M. Calligaro, H. E. Beere, and D. Ritchie, Appl. Phys. Lett. **87**, 071107 (2005).
[4] O. Gauthier-Lafaye, B. Seguin-Roa, F. H. Julien, P. Collot, C. Sirtori, J. Y. Duboz, and G. Strasser, Physica E (Amsterdam) **7**, 12 (2000).
[5] A. A. Belyanin, F. Capasso, V. V. Kocharovsky, Vl. V. Kocharovsky, and M. O. Scully, Phys. Rev. A **63**, 053803 (2001).
[6] A. Belyanin, C. Bentley, F. Capasso, O. Kocharovskaya, and M. O. Scully, Phys. Rev. A **64**, 013814 (2001).
[7] A. Kastalsky, IEEE J. Quantum Electron. **29**, 1112 (1993).
[8] J. Singh, IEEE Photonics Technol. Lett. **8**, 488 (1996).
[9] L. E. Vorobiev, JETP Lett. **68**, 417 (1998).
[10] M. Altarelli, U. Ekenberg, and A. Fasolino, Phys. Rev. B **32**, 5138 (1985).
[11] G. D. Sanders and Y. C. Chang, Phys. Rev. B **31**, 6892 (1985).
[12] U. Ekenberg, Phys. Rev. B **40**, 7714 (1989).
[13] C. Sirtori, C. Gmachl, F. Capasso, J. Faist, D. L. Sivco, A. L. Hutchinson, and A. Y. Cho, Opt. Lett. **23**, 1366 (1998).
[14] M. Rochat, L. Ajili, H. Willenberg, J. Faist, H. Beere, G. Davies, E. Linfield, and D. Ritchie, Appl. Phys. Lett. **81**, 1381 (2002).
[15] L. A. Kosi, H. Temkin, G. J. Pryzbylek, B. P. Segner, S. G. Napholtz, C. M. Bogdanowicz, and N. K. Dutta, Appl. Phys. Lett. **51**, 2219 (1987).
[16] L. Hvozdara, A. Lugstein, N. Finger, S. Gianordoli, W. Schrenk, K. Unterrainer, E. Bertagnolli, G. Strasser, and E. Gornik, Appl. Phys. Lett. **77**, 1241 (2000).
[17] *Introduction to Integrated Optics*, edited by M. K. Barnoski (Plenum Press, New York, 1974).
[18] S. O. Slipchenko, Z. N. Sokolova, N. A. Pikhtin, K. S. Bor-

schev, D. A. Vinokurov, and I. S. Tarasov, Semiconductors **40**, 990 (2006).
[19] L. A. Vainshtein, *Electromagnetic Waves* (Soviet Radio, Moscow, 1988) (in Russian).
[20] H. C. Casey and M. B. Panish, *Heterostructure Lasers* (Academic, New York, 1978), Parts A and B.
[21] L. D. Landau and E. M. Lifshitz, *Quantum Mechanics: Non-Relativistic Theory* (Elsevier Science, Burlington, 2003), Vol. 3, Chap. 3, p. 15.
[22] Ya. I. Khanin, *Fundamentals of Laser Dynamics* (Cambridge International Science Publishing, Cambridge, U.K., 2004).
[23] T. Elsaesser, J. Shah, L. Rota, and P. Lugli, Phys. Rev. Lett. **66**, 1757 (1991).
[24] A. Moskova and M. Mosko, Phys. Rev. B **61**, 3048 (2000).
[25] M. Hartig, J. D. Ganiere, P. E. Selbmann, B. Deveaud, and L. Rota, Phys. Rev. B **60**, 1500 (1999).
[26] O. Svelto, *Principles of Lasers* (Plenum Press, New York, 1989), Chap. 5.
[27] M. C. Tatham, J. F. Ryan, and C. T. Foxon, Phys. Rev. Lett. **63**, 1637 (1989).
[28] S.-C. Lee, I. Galbraith, and C. R. Pidgeon, Phys. Rev. B **52**, 1874 (1995).
[29] D. Bimberg, M. Grudmann, and N. N. Ledentsov, *Quantum Dot Heterostructures* (Wiley & Sons, New York, 1998).
[30] *Semiconductor Lasers*, edited by E. Kapon (Academic Press, San Diego, 1999).
[31] A. Yariv, *Introduction To Optical Electronics* (Holt, Rinehart and Winston, New York, 1976), Chap. 7.
[32] O. Kocharovskaya, P. Mandel, and Y. V. Radeonychev, Phys. Rev. A **45**, 1997 (1992).
[33] T. Ando, A. B. Fowler, and F. Stern, Rev. Mod. Phys. **54**, 437 (1982).
[34] S. Ghosh, Phys. Rev. B **62**, 8053 (2000).